Supporting Information: The impact of reaction rate on the formation of flow-driven confined precipitation patterns

Edina Balog,[a] Paszkál Papp,[a] Ágota Tóth,[a] Dezső Horváth,[b] and Gábor Schuszter*[a]

[a] *Department of Physical Chemistry and Materials Science, University of Szeged, Rerrich Béla tér 1., Szeged, H-6720, Hungary. E-mail: schuszti@chem.u-szeged.hu*

[b] *Department of Applied and Environmental Chemistry, University of Szeged*

March 30, 2020

Contents

1 Sketch of the Experimental Setup

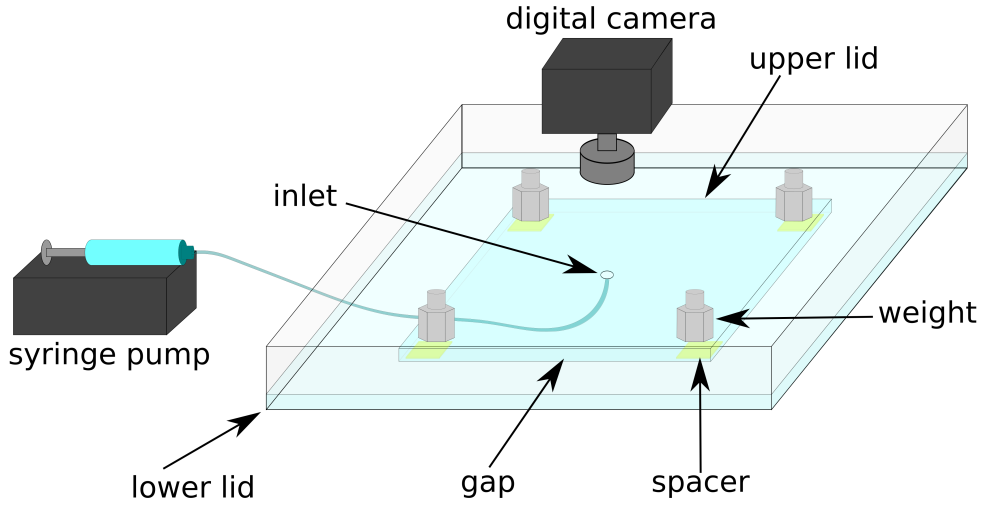

Figure 1: The horizontally oriented Plexiglas Hele–Shaw cell with 21×21 cm^2 practical reactor area. The lower and upper lids of the cell are separated by four tiny spacers (yellow squares) at the corners. Four weights (250 g each) placed above the spacers maintain constant gap height during injection. One reactant solution is filled in the gap prior the experiments while the other reactant solution is injected with a syringe pump from below through a tiny hole in the middle of the lower lid.

2 Solution Properties

Table 1: List of the solutions and their properties at 25 °C: density (ρ), dynamic viscosity (μ), pH, and the solubility product of the corresponding oxalate precipitate (K_{sp}).[1,2]

Solutions (0.25 M)	ρ / (g/cm^3)	μ / (mPa s)	pH	pK_{sp}
$MgCl_2$	1.0163	1.250	5.5	4.1
$CaCl_2$	1.0196	1.213	6.1	7.9
$SrCl_2$	1.0311	1.225	5.2	6.4
$BaCl_2$	1.0421	1.175	5.9	6.0
$CoCl_2$	1.0261	1.188	5.6	9.6
$NiCl_2$	1.0270	1.213	6.4	8.7
$CuCl_2$	1.0270	1.213	3.6	7.5
$ZnCl_2$	1.0267	1.150	5.9	8.9
$Na_2(COO)_2$	1.0236	1.288	6.8	-

3 Parameter Set of Hydrodynamic Simulations

The parameters used are taken to be similar to the experimental values corresponding to the Cu(II)-oxalate system (see Table 2). The volumetric flow rate (Q) set in the experiments is converted into linear flow velocity vector ($\vec{u}$) for the simulations. To investigate the saw-like precipitation patterns observed in experiments 5 min after the end of injection, $\vec{u}$ was estimated at 5 cm distance (r) from the inlet where the radial patterns appeared upon pumping in 5 mL solution. In this cylindrical region of the Hele-Shaw cell, $\vec{u}$ was calculated as

$$\vec{u} = \frac{Q}{2r\pi h},$$

where h is the height of the gap (0.5 mm). This way $Q = 20$ mL/min corresponds $\vec{u} = 2 \times 10^{-3}$ m/s.

A less negligible deviation between experimental and simulation parameters is the density difference of the injected and displaced solutions ($\Delta\rho$). Such value is set one order of magnitude higher than in experiments (i.e., 4.0×10^{-2} instead of 3.4×10^{-3} g cm^{-3}) to obtain clearly visible buoyancy stripes in the flow field. This discrepancy might be attributed to the fact that our model does not take precipitation into account, only the mixing of the two miscible liquids is considered. In the experiments, however, the appearance of a solid phase and thus the change of reactant concentration via chemical reaction leads to local density change in addition to the original $\Delta\rho$. To achieve qualitative agreement between experiments and simulations in future works, these effects must be considered. Applying a model grid with finer spatial resolution may improve the results as well.

Table 2: Parameter set used for hydrodynamic simulations: D, ρ, μ, $\vec{u}$, and g are diffusion coefficient, density, dynamic viscosity, linear flow velocity vector, and gravitational acceleration, respectively. M^{2+} represents the invading metal ion solution while A^{2-} stands for the displaced oxalate solution.

Parameter		Value	Unit
D	A^{2-}	1.9×10^{-9}	m^2 s^{-1}
	M^{2+}	2.0×10^{-9}	
ρ	A^{2-}	1.01	g cm^{-3}
	M^{2+}	1.05	
μ	A^{2-}	1.0	mPa s
	M^{2+}	1.0	
$\vec{u}$	i	10^{-3}	m s^{-1}
	ii	10^{-2}	
g		9.81	m s^{-2}

4 Concentration Profiles in Confined Geometry

Hydrodynamic simulations confirm that the injected liquid fills the entire gap in the vicinity of the inlet (Fig. 2) and that a parabolic concentration profile evolves during injection. Although there is a significant density difference between the solutions, the profiles appear identical independently of which solution is invading and which one is displaced. Unstable density stratification (i.e., more dense liquid on the top of the less dense one) is found in both cases, thus convective mixing is expected at the tip of the injected solution.

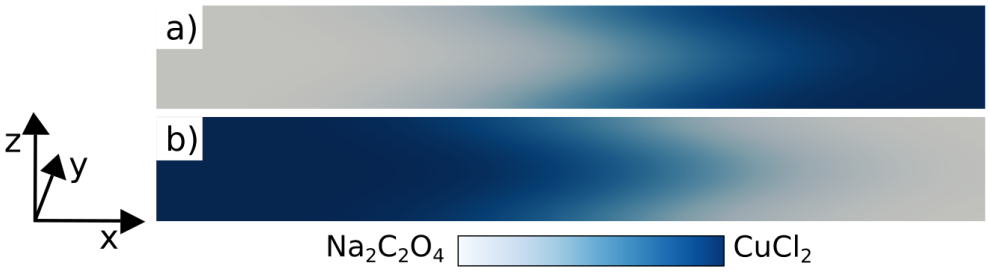

Figure 2: Vertical snapshots of simulations in the middle of the modelled reactor segment showing the concentration profile during direct (oxalate into Cu(II) solution; **a**) and reverse injections (Cu(II) into oxalate solution; **b**). For better visualisation, the aspect ratio is ten times enlarged along the z-axis; injection is along x-direction.

5 Spacing of Precipitate Stripes

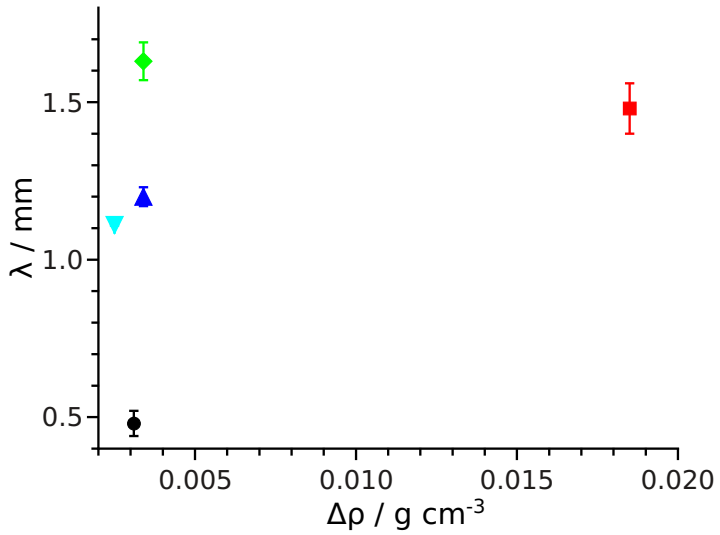

Figure 3: The spacing of precipitate stripes (λ) observed in different precipitation systems as a function of density difference between the injected and displaced solutions (Δρ) at Q=5 mL min^{-1} flow rate; Ba(II)–oxalate (■), Co(II)–oxalate (▼), Ni(II)–oxalate (▲), Cu(II)–oxalate (♦), and Zn(II)–oxalate (●).

6 Dissolution of $Cu(COO)_2$ Precipitation Patterns

The dissolution of $Cu(COO)_2$ precipitate is observed in oxalate excess because of the formation of dioxalatocuprate(II) complex. Even though the reactant concentrations are identical (0.25 M), the realisation of the experiment, i.e., that the oxalate solution is injected into the Cu(II) host solution provides such conditions that the already formed precipitate is surrounded by a large amount of oxalate ions. Therefore, the dissolution of crystals is present from the beginning of injection, but –because of kinetic reasons– becomes more pronounced upon waiting after the end of injection. Such dissolution is simultaneously tracked by following the amount of precipitate (gray scale intensity of images, I) and the area of precipitate covered rim of the pattern (A) as shown in Fig. 4.

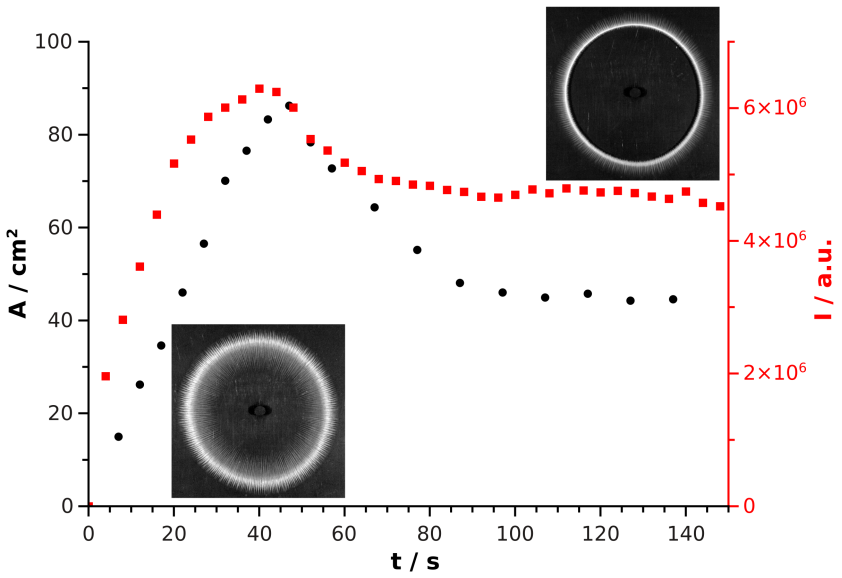

Figure 4: Dissolution of the $Cu(COO)_2$ precipitate tracked by monitoring the amount of precipitate (I; ■ corresponding to right axis) and the area of precipitate covered rim of the pattern (A; ● corresponding to left axis) with Q=5 mL min^{-1}.

In many experiments, the dissolution of the originally grown crystals was followed by recrystallisation, i.e., precipitate particles appeared with a new shape and size distribution. This effect is more pronounced at high oxalate excess and long reaction time, therefore demonstration experiments were performed by injecting 0.75 M oxalate solution into 0.25 M Cu(II) solution at Q=1 mL min^{-1} flow rate. The difference of the microstructures is shown in Fig. 5 for comparison. During injection, the pattern is composed of tiny and separated prism-like particles, while they recrystallise into significantly larger and needle-like structures. The recrystallisation can be further seen in the real time movie of ESI†. The identification of the chemical structure of the solid phases was not in the focus of our study but can be found in the literature.[3]

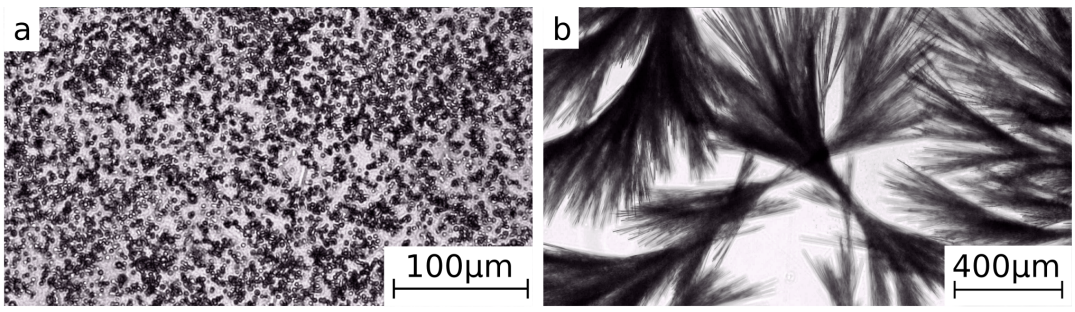

Figure 5: Representative precipitation particles observed during (a) and few minutes after injection (b) in the Cu(II)–oxalate system.

7 Movie

Real time experimental record taken with an optical microscope (Nikon Eclipse Ts2R coupled with a digital camera) at 4× magnification (field of view: 1.9×1.1 mm^2). The dissolution of tiny particles and the crystallisation of needle-like aggregates is shown after injecting 0.75 M oxalate solution into 0.25 M Cu(II) solution at Q=1 mL min^{-1} flow rate. The movie was taken at the pattern periphery once the injection stopped.

8 Comparison of the Amount of Precipitate in Different Reactions

To compare the amount of precipitate yielded in the different chemical systems during injection, the gray scale (I) of the experimental images is extracted and plotted as a function of time (t) in Fig. 6. Although the reflectance of different precipitate particles may strongly depend on their chemical character, size, and shape, such plots are frequently used to achieve rough estimates about the amount of product.[4,5] In this context, one can conclude that the alkaline earth metals produce less precipitate from calcium to barium and that the lowest amount of precipitate is found in the Cu(II) system.

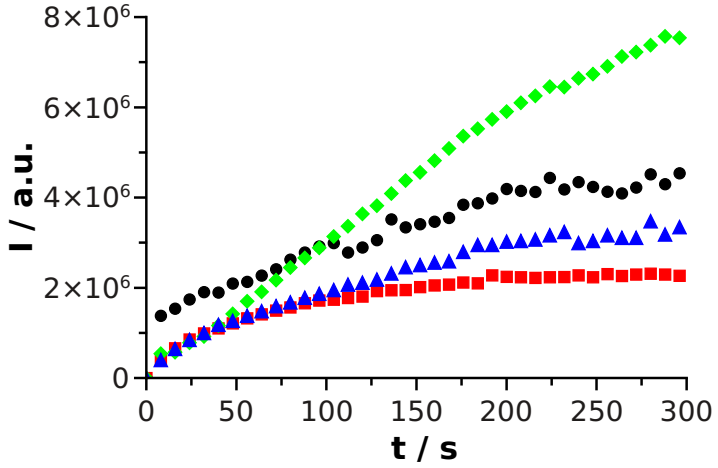

Figure 6: Gray scale (I) over time (t) during injection (Q=1 mL min^{-1}) for the different precipitation reactions: Ca(II)–oxalate (♦), Sr(II)–oxalate (●), Ba(II)–oxalate (▲), and Cu(II)–oxalate (■).

References

[1] S. Kotrlý and L. Šůcha, Handbook of Chemical Equilibria in Analytical Chemistry, Ellis Horwood Limited, England, **1985**.

[2] N.P. Das, B. Müller, Á. Tóth, D. Horváth, G. Schuszter, *Phys. Chem. Chem. Phys.* ***2018**, 20, 19768.*

[3] Á. Tóth, D. Horváth, Á. Kukovecz, M. Maselko, A. Baker, S. Ali, and J. Maselko, Pathway Control in the Self-construction of Complex Precipitation Forms in a Cu(II)–oxalate System, J. Syst. Chem. ***2012**, 3:4.*

[4] G. Schuszter, F. Brau, and A. De Wit, Flow-Driven Control of Calcium Carbonate Precipitation Patterns in Confined Geometry, Phys. Chem. Chem. Phys. ***2016**, 18, 25592.*

[5] F. Brau, G. Schuszter, and A. De Wit, Flow Control of A + B→C Fronts by Radial Injection, Phys. Rev. Lett. ***2017**, 118, 134101.*